Au@Ag Nanoparticles: Halides Stabilize {100} Facets

ARTICLE *in* JOURNAL OF PHYSICAL CHEMISTRY LETTERS · JUNE 2013

Impact Factor: 7.46 · DOI: 10.1021/jz401269w

THE JOURNAL OF PHYSICAL CHEMISTRY Letters

Letter

pubs.acs.org/JPCL

Au@Ag Nanoparticles: Halides Stabilize {100} Facets

Sergio Gómez-Graña,[†] Bart Goris,[‡] Thomas Altantzis,[‡] Cristina Fernández-López,[†] Enrique Carbó-Argibay,[†] Andrés Guerrero-Martínez,[†,§] Neyvis Almora-Barrios,[∥] Nuria López,[∥] Isabel Pastoriza-Santos,[†] Jorge Pérez-Juste,[†] Sara Bals,[‡] Gustaaf Van Tendeloo,[‡] and Luis M. Liz-Marzán*[,†,⊥,#]

[†]Departamento de Química Física, Universidade de Vigo, 36310 Vigo, Spain

[‡]EMAT-University of Antwerp, Groenenborgerlaan 171, B-2020 Antwerp, Belgium

[§]Department of Physical Chemistry I, Complutense University of Madrid, Avenida Complutense s/n, 28040 Madrid, Spain

[∥]Institute of Chemical Research of Catalonia, ICIQ, Avinguda Països Catalans, 16, 43007 Tarragona, Spain

[⊥]BioNanoPlasmonics Laboratory, CIC biomaGUNE, Paseo de Miramón 182, 20009 Donostia - San Sebastián, Spain

[#]Ikerbasque, Basque Foundation for Science, 48011 Bilbao, Spain

Supporting Information

ABSTRACT: Seed-mediated growth is the most efficient methodology to control the size and shape of colloidal metal nanoparticles. In this process, the final nanocrystal shape is defined by the crystalline structure of the initial seed as well as by the presence of ligands and other additives that help to stabilize certain crystallographic facets. We analyze here the growth mechanism in aqueous solution of silver shells on presynthesized gold nanoparticles displaying various well-defined crystalline structures and morphologies. A thorough three-dimensional electron microscopy characterization of the morphology and internal structure of the resulting core−shell nanocrystals indicates that {100} facets are preferred for the outer silver shell, regardless of the morphology and crystallinity of the gold cores. These results are in agreement with theoretical analysis based on the relative surface energies of the exposed facets in the presence of halide ions.

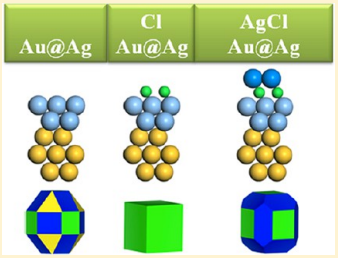

SECTION: Plasmonics, Optical Materials, and Hard Matter

Geometry control of metal particles at the nanoscale is a crucial step in the development of nanoplasmonic materials and devices.[1,2] Among all the reported synthetic routes, the seeded growth method can be considered as the most versatile one, since it allows fine-tuning of both the morphology and size of the nanoparticles by simply reducing additional metal ions on preformed nanoparticle seeds.[3,4] Such seeded growth process can be implemented either in aqueous solution or in organic solvents such as *N*,*N*-dimethylformamide (DMF) or polyols,[5] usually mediated by surfactants or polymers, respectively.[6] Typically, reduction in organic solvents (which are the actual reducing agents) requires different experimental conditions, such as higher temperatures or the presence of (apparently) spectator ions. Although both approaches cannot be easily compared, it is widely accepted that the final particle shape, regardless of the synthetic approach, is mainly dictated by the crystalline structure of the seed, as well as by the effect of ligands (surfactants/polymers) and other additives (ions in general). The preferential adsorption of ligands or additives onto the seeds makes certain crystallographic facets thermodynamically more stable, reducing their surface free energy. As a consequence, the relative free energies for different facets and thus their relative growth rates may change as compared to surface energies in vacuum. Although the fast development of spectroscopic techniques has allowed us to learn progressively more about the growth mechanism, the explicit role of the different additives has not been unequivocally discerned. In nonaqueous solvents, seed-mediated growth has been widely explored for silver, gold, and other metals, allowing in each case to propose a possible growth mechanism.[4,7,8] However, in aqueous solution, the method has been mainly developed to generate gold nanoparticles in a wide range of morphologies, including Platonic solids, prisms, and other shapes containing high-index facets.[3] Different approaches have also been recently proposed for silver nanoparticles,[9−15] although shape-controlled synthesis still requires deeper insights in this case. Focusing on the seeded growth approach in aqueous media, control over particle growth has been achieved in the presence of surfactants (most frequently cetyltrimethylammonium bromide, CTAB) containing halides and silver ions as key additives. Generally, the detailed analysis of the growth process and the crystalline structure of the particles have been used to help establish the corresponding growth mechanisms.[16] A general method has been recently proposed to explain the shape evolution of small

Received: June 19, 2013
Accepted: June 20, 2013
Published: June 20, 2013

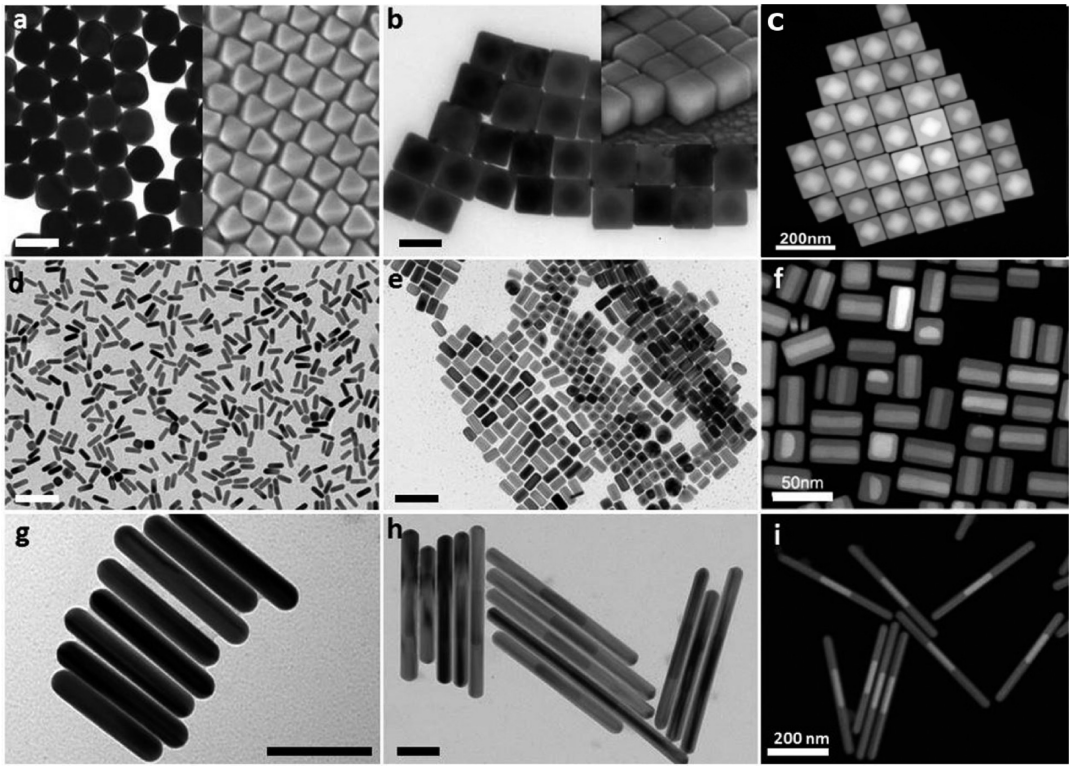

Figure 1. Representative TEM and SEM images of the different gold nanoparticles used as seeds (left column, scale bars: 100 nm) and the corresponding Au@Ag counterparts after silver growth (middle column, scale bars: 100 nm). The right column displays HAADF-STEM images of the same core−shell particles, where the silver shells can be easily discerned from the gold cores.

spherical and single crystalline gold nanoparticles in aqueous surfactant solutions.[17] This work focused on the influence of halide ions, either in the absence or in the presence of silver ions, on gold overgrowth, and different types of growth mechanisms were proposed: (i) a kinetically controlled mechanism in the absence of silver ions, (ii) a silver underpotential deposition (Ag UPD) mechanism based on the interaction of silver with the surface of gold particles, or (iii) a Ag UPD mechanism influenced by the concentration and type of halide ions. In most cases, the overgrown particles were single crystalline and they could present higher or lower index facets depending on the growth mechanism.

In this context, we decided to accomplish the understanding of silver deposition on preformed gold nanoparticles with well-defined crystalline structure and lateral facets, so as to establish the key parameters that govern the seeded growth mechanism and eventually the shape and crystallinity of the resulting core−shell particles. Our results provide evidence behind the preferential formation of Ag {100} facets regardless of the starting morphology, which are stabilized by halide ions as predicted by density functional theory (DFT) surface energy calculations. We selected for this study three different types of gold nanoparticles, which feature different lateral facets. Whereas single crystal octahedrons (Figure 1a) are surrounded by eight {111} facets,[7] single crystal nanorods have an octagonal cross section featuring eight {520} lateral facets and a combination of {110} and {111} facets at the tips,[18,19] and pentatwinned nanorods display five {100} lateral facets and five {111} facets at each tip.[20] Silver coating was carried out following a modification of the procedure recently reported by Vaia and co-workers.[14] Although the method was reported for nanorods, the same procedure was adapted for coating octahedra as well. In all cases, the seeds (0.25 mM Au^0) were added to a growth solution containing benzyldimethylhexadecylammonium chloride (BDAC) (10 mM), $AgNO_3$ (1 mM) and ascorbic acid (4 mM). Silver deposition was carried out at relatively low surfactant concentration (10 mM BDAC), which determines that the silver precursor is AgCl as proposed in ref 14, ascorbic acid being the reducing agent. The process was carried out at 60 °C to ensure controlled silver reduction. Figure 1 shows representative transmission electron microscopy (TEM) and scanning electron microscopy (SEM) images of the three different gold nanoparticle seeds employed, as well as the corresponding particles obtained upon silver seeded growth. A high-angle annular dark field scanning TEM (HAADF-STEM) image of each type of core−shell nanoparticles is also included. Since HAADF-STEM images yield intensities that scale with the atomic number *Z*, the silver shells can be easily discerned from the gold cores (brighter in the dark field images).

It can be observed that silver coating results in different morphologies for the various types of Au nanoparticle seeds, which might be related to the initial differences in anisotropy, which are somehow preserved in the core−shell particles, as previously reported.[15] However, proper understanding of the growth mechanism requires a detailed separate study for each particular case, which we carried out by means of high resolution transmission electron microscopy (HRTEM) and HAADF-STEM electron tomography. Such an analysis allowed us to accurately establish the corresponding morphologies, crystalline structures, and index of the different facets for both the cores and shells. This information, together with the well-defined structure of the gold seeds and theoretical modeling was ultimately used to propose a common mechanism for silver deposition on gold nanoparticles (see below). For simplicity,

dx.doi.org/10.1021/jz401269w | *J. Phys. Chem. Lett.* 2013, 4, 2209−2216

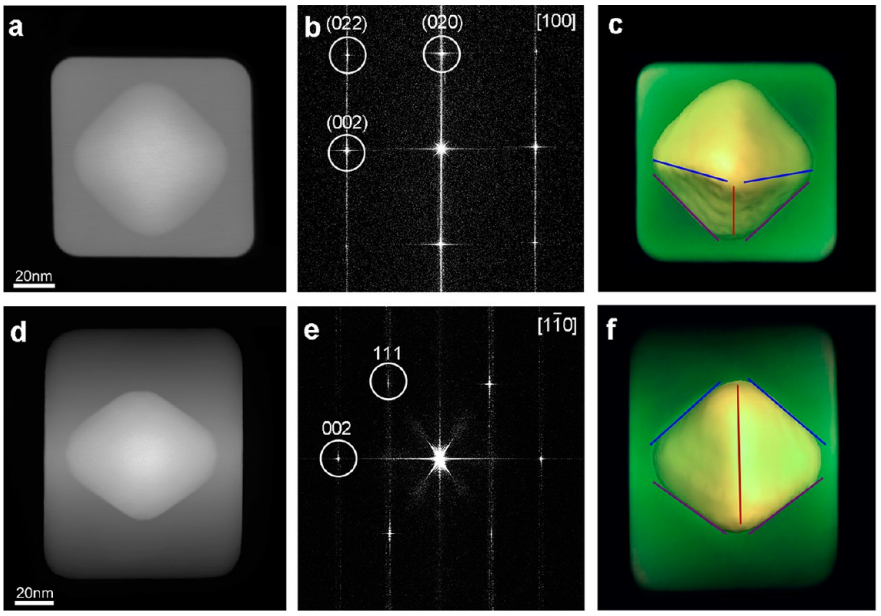

Figure 2. Upper panels: (a) High-resolution HAADF-STEM image of an Au@Ag particle. (b) The corresponding FFT of the image in a, showing that the outer facets of the cube are {100} planes. The absence of splitting on the diffraction spots reveals epitaxial growth of silver on gold. (c) Visualization of the 3D reconstruction of the particle shown along the same direction as presented in a. Lower panels: (d) High-resolution HAADF-STEM image of the particle in a, rotated over 45° along the [001] zone axis. (e) The corresponding FFT of the image in d, showing that the facets of the octahedron are {111} planes. (f) Visualization of the 3D reconstruction of the particle shown along the same direction as presented in d. The arrangement of the Au octahedron inside the silver cube is confirmed from these experiments.

we present a separate discussion for growth on single crystalline and pentatwinned seeds.

The two types of single crystalline seeds selected for this work differ not only in their morphology (octahedra vs nanorods), but also in the crystalline indices of their external facets. Whereas octahedra are highly isotropic and enclosed by eight {111} facets, nanorods display high anisotropy and are enclosed by eight {520} lateral facets along a (100) zone axis.[18,19] Figure 1a shows a representative TEM image of the gold octahedra used as seeds, with an average side length of ca. 60 nm. Although the TEM projections of the particles seem to indicate a hexagonal cross section, this is a consequence of the octahedral shape, which was confirmed by SEM. Upon silver growth, TEM images suggest that the coated particles present a square cross section, with an average side length of 102 nm (Figures 1b and S1 in the Supporting Information). The inset in Figure 1b and Figure S1 show representative SEM images in which indeed the cubic morphology of the grown nanoparticles can be readily elucidated.

Although TEM allows us to discern the presence of the octahedral cores inside the silver cubes, additional characterization by high-resolution HAADF-STEM imaging was required to investigate in detail the core−shell interfaces and crystalline structure (Figure 2a). Since the signal in HAADF-STEM mode depends on the atomic number of the elements, it is obvious that the brighter inner region corresponds to the Au octahedron (square projection in Figure 2a) and the darker outer area corresponds to the silver shell. The corresponding fast Fourier transform (FFT) of the image reveals the absence of splitting in the diffraction spots, thereby confirming that silver has grown epitaxially on the gold surface (Figure 2b). Electron tomography was used to obtain a three-dimensional visualization of the particles as shown in Figure 2c. The three-dimensional (3D) image shows that the gold octahedron is surrounded by a silver cube, and the six vertices of the inner octahedron are pointing at the six faces of the outer cube (Figure 2c). The FFT of the particle in the [100] zone axis (see Figure 2b) shows that the six faces of the silver cube are of the {100} type, as expected. Rotating the same particle 45° along the [001] axis (Figure 2d−f), allowed us to also index the facets of the inner gold octahedron. The FFT of the HRSTEM image shows that the octahedron is enclosed by {111} facets. Similar results were obtained by analyzing the selected area electron diffraction pattern of the bright-field TEM images of the same particle oriented along the [001] zone axis (see Figure S2, Supporting Information).

A similar analysis was carried out on single-crystal nanorods coated with silver, synthesized through seeded growth on single crystalline gold seeds.[21] This synthesis yields rather monodisperse nanorods (see Figure 1d), which have been reported to have an octagonal cross section and eight high index {520} lateral facets.[18,19] The overview TEM image of the silver-coated nanorods (Figure 1e) indicates that some particles exhibit a projection with a rectangular shape, but a closer look at the image reveals also the presence of particles that are standing perpendicular to the TEM grid, with a square cross section as previously reported for similar syntheses.[14,15,22] Additionally, the HAADF-STEM image in Figure 1f provides a much better contrast and allows a clear distinction between the Au nanorod core and the silver shell. A representative TEM image of a particle lying on the grid with its corresponding electron diffraction pattern is shown in Figure S3 (Supporting Information). The diffraction pattern indicates that the coated nanorod is oriented along a [100] zone axis and the absence of spot splitting again indicates epitaxial growth of Ag on the Au nanorod. This information demonstrates that the external silver shell provides an overall square prismatic morphology, and is thus enclosed by six {100} facets.

HRTEM analysis of standing nanorods allowed us to index the lateral facets of both the nanorod core and the external Ag

dx.doi.org/10.1021/jz401269w | J. Phys. Chem. Lett. 2013, 4, 2209−2216

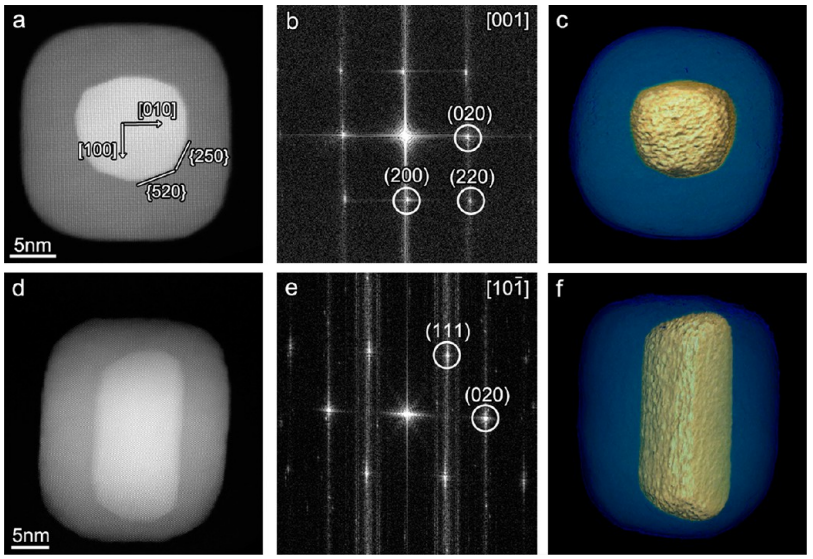

Figure 3. Upper panels: (a) High-resolution HAADF-STEM projection of an Au@Ag nanorod standing perpendicular to the carbon support. (b) FFT of projection a, revealing that the external facets of the Ag shell are of the {100} type. (c) 3D rendering of the tomographic reconstruction of the same nanorod, shown along the same viewing direction as the HAADF-STEM projection. Lower panel: (d) High-resolution HAADF-STEM projection of the same nanorod rotated over 90°. (e) FFT projection of d. (f) 3D rendering parallel to the long axis of the nanorod ([110] direction).

shell (Figure 3). The corresponding FFT patterns confirm that the crystalline facets of the external Ag shell are of the {100} type. Regarding the core, although the octagonal cross section is not perfectly defined, it is clear from the HRTEM image that the corners or smaller faces are in coincidence with the [100] and [110] directions, while the side facets can indeed be assigned to the {520} family, in accordance with previous results. These observations are further confirmed by 3D reconstructions at the atomic scale, which will be reported elsewhere. Additional TEM analysis shows that silver coating induces the transformation of the Au octagonal prism into an Au@Ag square prism with six {100} facets, on which silver deposition occurs uniformly for all six facets, leading to a gradual decrease in the aspect ratio, eventually leading to transformation of the prisms into cubes.[23] Figure S4 in the Supporting Information shows an example in which seeded growth with increasing amounts of silver leads to a decrease of the overall aspect ratio of the particles from 3.9 to 1.2.

Pentatwinned gold nanorods have a well-defined crystalline structure, generated by the propagation of the five twin boundaries along the growth direction of the nanorods. These nanorods are synthesized by seed mediated growth, through reduction of $HAuCl_4$ with ascorbic acid in the presence of citrate-capped pentatwinned seeds and CTAB, and are typically longer (higher aspect ratios) than single crystal rods (Figure 1g).[24] It has been reported that the twinned structure of the seed determines the twinning of the grown nanorods,[25] leading to a pentagonal prism morphology enclosed by five {100} lateral facets and terminated by 10 {111} tip facets.[20] Coating of pentatwinned nanorods was carried out under similar experimental conditions as those for the single crystalline gold seeds, but a rather different morphology was revealed by the TEM images (see Figures 1h,i and 4a). The contrast between Au and Ag allows us to see that, in this case, the deposition of Ag atoms preferentially occurs at the tips of the nanorods, thus increasing their aspect ratio, while the initial gold particle remains at the center of the resulting Au@Ag nanorod. We found that the aspect ratio of the resulting core−shell nanorods can be controlled by simply varying the ratio between silver nitrate and Au nanorod seeds in the growth process (see Figure S5 in the Supporting Information). Further analysis was carried out to disclose the structure of the Au@Ag nanorods. Figure 4a shows an overview HAADF-STEM image of Au@Ag pentatwinned nanorods. The inset in this figure presents the projection of a standing Au@Ag nanorod, where one can nicely distinguish an inner and brighter pentagon, which reflects the pentagonal cross section of the Au nanorod core. Additionally, a darker, concentric pentagonal corona can be also appreciated that corresponds to the silver shell. Although the Ag shell seems to be deposited in an epitaxial manner, unfortunately, the length of the core−shell nanorod did not allow us to obtain a HRTEM image in this orientation. Further evidence of epitaxial growth was provided by the absence of splitting in the spots of the FFT patterns of two selected areas located at opposite sides of a core−shell nanorod (see Figure 4b). The FFT patterns shown in Figure 4d,e also indicate that these pentatwinned Au@Ag nanorods are oriented in both the ⟨110⟩ and ⟨111⟩ zone axes, and therefore only at the right side is the {100} facet actually parallel to the electron beam. This is illustrated by the model shown in Figure 4c. Thus, Ag deposition seems to involve growth on the {111} tip facets and thus stabilization of the {100} lateral facets. Therefore, contrary to what was found for the coating of single crystalline Au nanorods, the seeded growth of pentatwinned Au nanorods results in an increase of the aspect ratio and, therefore, increased anisotropy, in agreement with other recent indications.[15]

Proposing a growth mechanism based on the results reported in this manuscript requires taking into account the various parameters that may influence the final particle morphology. First of all, the experimental conditions were found to be crucial for a homogeneous growth of the particles, in particular the silver complex precursor and the reaction temperature. Second, the crystalline structure of the seed ultimately dictates the shape evolution upon growth.

Silver Precursor. Typically the silver precursor for the aqueous synthesis of Ag or Au@Ag core−shell nanoparticles is $AgNO_3$.

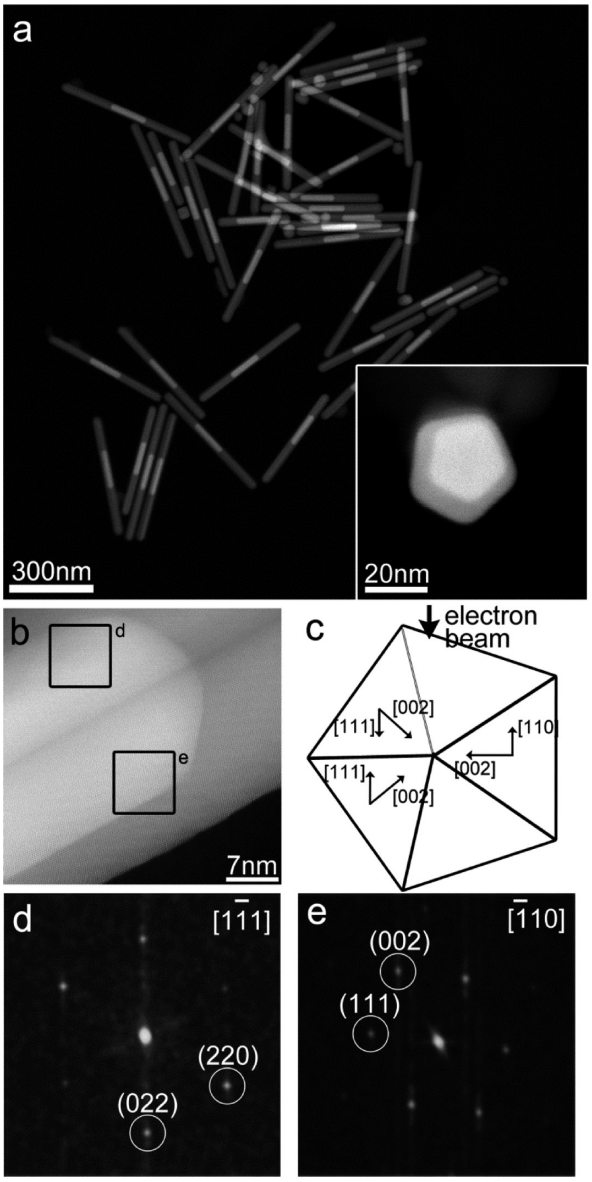

Figure 4. (a) Representative HAADF-STEM image of Au@Ag core–shell pentawinned nanorods. The inset shows a HAADF-STEM image of a standing Au@Ag nanorod. (b) High-resolution HAADF-STEM projection of a Au@Ag pentatwinned nanorod showing the crystalline structure of the nanorod. (d,e) Fourier transforms of the regions indicated in b, which indicate that the left side corresponds to a ⟨111⟩ zone axis, whereas the right side corresponds to a ⟨110⟩ zone axis. These FFT patterns are consistent with a pentagonal cross section of the nanorod as shown in c.

In the presence of surfactants, such as CTAB or BDAC, the bromide or chloride counterions may lead to the formation of insoluble AgBr or AgCl, which however can be avoided by increasing the surfactant concentration. While at 2:1 molar ratio of CTAB to $AgNO_3$ silver bromide crystals are formed (as indicated by the turbidity of the suspension[26]), at a molar ratio of 500:1 (Ag^+ concentration fixed at 0.1 mM) solubilization of AgBr occurred due to the formation of AgBr/CTAB complexes.[27] In the present case, we are dealing with a molar ratio of 10:1, which allows using a much higher Ag^+ concentration (1 mM) and therefore growth of thicker Ag shells. At this intermediate ratio, the formation of insoluble AgBr/AgCl species will be time dependent (and also temperature dependent, see below) as reported by Vaia and co-workers.[14] Interestingly, we have found better reproducibility and less free nucleation using BDAC when compared to CTAB. This can be ascribed to the slower nucleation of AgCl nanocrystals versus that of AgBr (solubility products are 1.8×10^{-10} and 5.0×10^{-13}, respectively).

Reducing Agent. Ascorbic acid has been demonstrated to be a versatile reducing agent for the aqueous synthesis of gold and silver nanoparticles. However, in the case of silver, the redox potential of ascorbic acid is not sufficient to reduce Ag^+ to Ag^0 at "normal conditions", i.e., room temperature and pH 7. The reducing power of ascorbic acid can be tuned by varying pH or temperature. For instance, the catalytic reduction of silver ions on preformed silver or gold nanoparticles has been observed to occur when the pH was increased from 7 to 9–10.[28] Nevertheless, the pH threshold is quite narrow, and the reduction rate increases significantly (the reduction is complete within a few minutes), giving rise to irregular growth and eventually to nucleation in solution.[13,14,29] Temperature has also been reported to affect the redox potential of ascorbic acid, but to a smaller extent.[30,31] At room temperature and ascorbic acid to silver nitrate ratio of 4:1, silver ions cannot be reduced on the gold seeds, but if the temperature is raised to 60 °C, reduction proceeds at a slow reduction rate (the reduction is completed within 3 h).

Crystallinity of the Au Seeds. Our results for seeded growth on monocrystalline gold seeds, both octahedrons (enclosed by eight {111} facets) and nanorods (enclosed by eight {520} lateral facets), show that silver deposition leads to the formation of {100} Ag facets. As a consequence, Au octahedrons transform into cubes, which subsequently grow uniformly so that the cube dimensions increase. During the shell growth on nanorods, silver deposition was found to occur preferentially on the {100} facets, both on side and tip facets, so that rectangular prisms are obtained, and then preferential (or faster) growth occurred on the lateral facets (see Figure S4, Supporting Information). This preferential lateral growth might be driven simply by a tendency to decrease the surface area when anisotropy is decreased. On the other hand, silver deposition on pentatwinned nanorods (five {100} lateral facets and five {111} facets at each tip) seems to proceed through a completely different mechanism, since the aspect ratio gradually increases and the pentatwinned structure is preserved. In fact, this finding opens up new possibilities for tailoring the aspect ratio of Ag nanorods and nanowires (see Figure S5, Supporting Information). Such an increase in aspect ratio effectively means that {111} facets are still present at the tips (with only slightly larger size than in the initial rods) while the {100} lateral facets get increasingly larger.

Taking all these considerations into account, we propose a growth mechanism in which the final nanoparticle morphology is achieved through a combination of kinetic control and surface stabilization of the {100} facets, facilitated by halide/surfactant adsorption. The kinetic control implies a slow reduction of the silver precursor, which is essential to allow differences in the surface energy of the different facets, in this way favoring the growth of more thermodynamically favorable particle shapes. Further evidence behind the discussion above is provided by theoretical calculations of surface energies. DFT-based simulations were performed for the adsorption of different chloride structures on a model system formed by a gold substrate with different orientations—(111), (100), and (110)—that has been epitaxially coated by two monolayers of

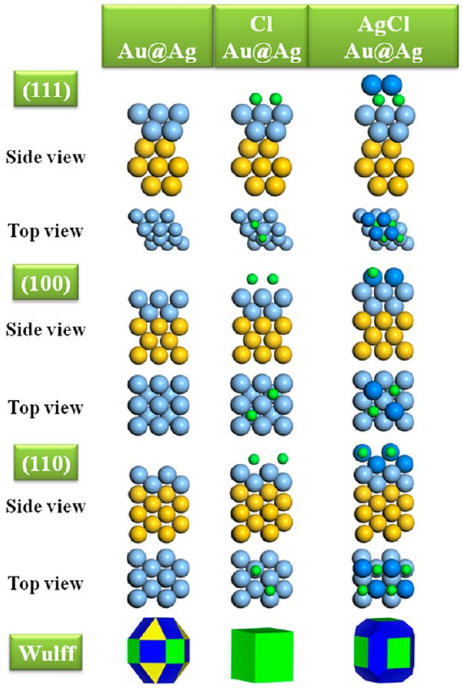

Figure 5. Calculated surface stuctrures for different facets: (111), (100), (110), and different surface terminations. Left column: two silver monolayers on gold Au@Ag(2 ML); central column: Cl adsorption in a dense phase; right column: AgCl growth on Au@Ag(2 ML). In each case, the termination of AgCl follows that of the substrate. Color code: golden Au, blue Ag, dark blue Ag^+, green Cl or Cl^-. The bottom row shows the corresponding Wulff (equilibrium) structures: yellow planes are {111}, green planes are {100}, and blue planes are {110} facets.

silver (see Figure 5). The surface energies, γ, for the clean facets follow the order (111) < (100) < (110) (see Table S1, Supporting Information). Chlorine adsorption has been reported to result in the formation of dense chlorine structures.[32] Our results show that Cl atoms favorably adsorb on Ag by about 1 eV on (111) faces but can form even denser structures on (100) facets, resulting in a stronger interaction of 1.6 eV/Cl. This energy is saturated, as no further energy gain is obtained on more open planar surfaces such as the (110). Calculated energy changes for Cl adsorption on equivalent Au structures is smaller, such as 1.1 eV/Cl atom, for the (100) facet. This large energy gain reduces the adsorbate-modified surface energy, $\gamma' = \gamma + \Delta E/A$ (ΔE is the interaction energy, A is the surface area), and, as a consequence, (100) facets show the lowest surface energy γ' (Table S2, Supporting Information). Moreover, there is enough room in the superstructure to accommodate Ag ions in the form of a surface chloride phase, in which Ag and Cl atoms are placed on the surface following the termination of the substrate. This implies a polar termination for AgCl on Ag following the {111}||{111} alignments, and {100}||{100} and {110}||{110} with nonpolar terminations for AgCl (see Figure 5). As nonpolar terminations are less energy demanding, the resulting structures show lower γ' (see Table S2). Surface energies can be employed to build the nanoparticle with minimum surface energy, i.e. thermodynamically controlled, through Wulff construction.[33,34] As shown in the bottom row of Figure 5, for the Au@Ag clean model, the constructed nanoparticle shows all the considered {111} planes, but when Cl^- is adsorbed, the structure mainly contains {100} facets, in agreement with the experiments described in Figures 1−4. Wulff construction also indicates that intermediates with AgCl structures would mainly show {100} and {110} facets.

In summary, we have demonstrated that the slow reduction of silver ions, in the presence of BDAC as stabilizer, on presynthesized gold nanoparticles with well-defined crystalline structures and different outer facets, leads to the preferential growth of Ag {100} facets, which is not in full agreement with the general sequence of surface energies for the different crystallographic fcc planes. However, the surface energies of the different facets can be significantly affected by the adsorption of different chemical species such as halide ions, as confirmed by DFT calculations of surface energies. This effectively explains why single crystalline gold nanoparticles such as octahedra and nanorods evolve into single crystalline Au@Ag cubes enclosed by six {100} facets, while pentatwinned gold nanorods evolve into core−shell nanorods with an increased aspect ratio, since the seed particles display five {100} lateral facets, which get extended in the seeded growth process.

EXPERIMENTAL DETAILS

Chemicals. Ascorbic acid, $HAuCl_4 \cdot 3H_2O$, $AgNO_3$, $NaBH_4$, cetyltrimethylammonium bromide (CTAB), benzyldimethylhexadecylammonium chloride (BDAC), HCl (37%), trisodium citrate and butenoic acid were purchased from Sigma-Aldrich. All chemicals were used as received. Milli-Q grade water was used as solvent.

Gold Nanoparticle Synthesis. Single Crystal Gold Nanorods: AuNRs were prepared by the Ag^+-mediated seeded growth method.[21] Seed solutions were made by mixing a CTAB solution (4.7 mL, 0.1 M) with 25 μL of 0.05 M $HAuCl_4$; we kept this solution at 30 °C for 5 min and then 300 μL of sodium borohydride was added quickly under vigorous stirring. The resulting solution was stored at 30 °C. An aliquot of the seed solution (24 μL) was added to a growth solution (10 mL) containing CTAB (0.1 M), $HAuCl_4$ (0.5 mM), ascorbic acid (0.8 mM), and $AgNO_3$ (0.08 mM). The reaction beaker was stored at 30 °C overnight. AuNRs were then washed by 2-fold centrifugation (8500 rpm, 25 min), the supernatant was discarded and the precipitate was redispersed in a 10 mM BDAC solution. *Pentatwinned Gold Nanorods:* Pentatwinned AuNRs were prepared following a previously reported seeded growth method.[24,35] The seed solution (gold spheres of ca. 3.5 nm diameter) was prepared as follows: 20 mL of an aqueous solution containing 0.125 mM $HAuCl_4$ and 0.25 mM trisodium citrate was prepared in a beaker, to which 0.3 mL of freshly prepared 0.01 M $NaBH_4$ solution was added under vigorous stirring. After 30 s, stirring was slowed down, and the colloidal dispersion was stored between 40 and 45 °C for 15 min to ensure decomposition of excess $NaBH_4$. In a second step, the seeds were grown to 5.5 nm as follows: 5 mL of growth solution consisting of 1.25×10^{-4} M $HAuCl_4$ and 0.04 M CTAB at 25−30 °C was mixed under stirring with 0.0125 mL of 0.1 M ascorbic acid. Subsequently, 1.67 mL of the 3.5 nm Au-citrate seed solution was quickly added while stirring. In the last step, pentatwinned AuNRs were grown. Briefly, 0.625 mL of 0.1 M ascorbic acid was added to 250 mL of a growth solution ($[HAuCl_4]$ = 0.125 mM; [CTAB] = 8 mM) at 20 °C. Upon homogenization, 750 μL of 5.5 nm Au-CTAB seed solution was added and allowed to react for several hours. As a result, a mixture of spheres, plates, and rods was obtained. The gold nanorods were separated as reported by Jana.[36] A total

volume of 250 mL was centrifuged at 6500 rpm for 10 min, the supernatant was discarded, and the precipitate was redispersed in CTAB 0.1 M. The samples were concentrated again by centrifugation (10 min at 6500 rpm), and the concentrated sample (4 mL) was first heated at 50 °C for 5 min and then cooled down. After cooling, the precipitate was collected and redispersed in 9 mL of water. *Gold Octahedrons:* Gold octahedrons were prepared by seeded growth from single crystal Au nanorods (58 nm long). The growth solution was prepared mixing 50 mL of BDAC (10 mM) with 500 μL of $HAuCl_4$ (0.05 M), and 221 μL of butenoic acid was added to reduce the Au^{3+} to Au^{+}. The solution was kept at 30 °C until the yellow color disappeared (20 min) and then 825 μL of washed Au nanorods was added as seeds; the beaker was stored at 30 °C for 2 h. Gold octahedrons were washed by centrifugation (3500 rpm, 20 min), the supernatant was discarded and the precipitate redispersed in a solution of BDAC 10 mM.

Silver Overgrowth. Silver coating was carried out following a modification of the procedure previously reported by Vaia and co-workers.[14] Regardless of the morphology of the gold nanoparticles used as seeds, a growth solution (5 mL) was prepared containing 10 mM BDAC, 1 mM $AgNO_3$, 4 mM ascorbic acid and 0.25 mM Au^0 (as the corresponding gold nanoparticles). After the last addition, the temperature was increased up to 60−65 °C and maintained for 3 h. Finally, the obtained solution was centrifuged (6000 rpm 20 min) and redispersed in water.

Characterization Techniques. Optical characterization was carried out by UV/vis spectroscopy with either Agilent 8453 or Cary 5000 spectrophotometers. TEM images were obtained with a JEOL JEM 1010 transmission electron microscope operating at an acceleration voltage of 100 kV. SEM images were obtained using a JEOL JSM-6700F FEG scanning electron microscope operating at an acceleration voltage of 5.0 kV for secondary-electron imaging (SEI). Tilt series for 3D tomography were acquired using a FEI Tecnai G2 microscope, operated at 200 kV. A single tilt tomography holder (Fishione model 2020) was used for acquisition, and the alignment and reconstruction were carried out using the FEI Inspect3D software. HAADF-STEM images were acquired using a double aberration corrected Titan 50−80 microscope operating at 300 kV in STEM mode.

Computational Approach. Surface energies were calculated on slab models representing low index surfaces with the VASP code.[37] The functional of choice was PBE (Perdew, Burke, Ernzerhof),[38] and PAW (Projector Augmented Wave)[39] was employed to replace the inner electrons, while the valence monoelectronic states were expressed in plane waves with a 450 eV cutoff. The slab models contain at least three gold layers and two outermost Ag layers were placed on top. Slabs were interleaved by at least 12 Å, and the spurious dipole arising from the asymmetric configuration of the slab was removed.[40] The procedure follows that in ref 34. Different reconstructions for the surface terminations were employed, but, in general, (2 × 2) supercells were found sufficient for the present process. Cl^- adsorption was obtained via a Born-cycle as described in ref 41 and including the solvation terms from Gibbs free energy.[42]

■ ASSOCIATED CONTENT

Ⓢ Supporting Information

Additional TEM and SEM images, electron diffraction patterns, and dimensions of Au@Ag nanocrystals. Tables of calculated surface and adsorption energies. This material is available free of charge via the Internet at http://pubs.acs.org

■ AUTHOR INFORMATION

Notes

The authors declare no competing financial interest.

■ ACKNOWLEDGMENTS

This work has been funded by the European Research Council (ERC Advanced Grant #267867 Plasmaquo, ERC Advanced Grant 24691 Countatoms). L.M.L.-M., G.V.T., and S.B. acknowledge funding from the EU (ESMI, FP7-INFRASTRUCT-2010-1, Grant #262348). B.G. acknowledges financial support by the Flemish Fund for Scientific Research (FWO). We thank BSC-RES for providing us with generous computational resources.

■ REFERENCES

(1) Alvarez-Puebla, R. A.; Liz-Marzán, L. M.; García de Abajo, F. J. Light Concentration at the Nanometer Scale. *J. Phys. Chem. Lett.* **2010**, *1*, 2428−2434.

(2) Mahmoud, M. A.; El-Sayed, M. A. Different Plasmon Sensing Behavior of Silver and Gold Nanorods. *J. Phys. Chem. Lett.* **2013**, *4*, 1541−1545.

(3) Grzelczak, M.; Pérez-Juste, J.; Mulvaney, P.; Liz-Marzán, L. M. Shape Control in Gold Nanoparticle Synthesis. *Chem. Soc. Rev.* **2008**, *37*, 1783−1791.

(4) Xia, Y.; Xiong, Y.; Lim, B.; Skrabalak, S. E. Shape-Controlled Synthesis of Metal Nanocrystals: Simple Chemistry Meets Complex Physics? *Angew. Chem., Int. Ed.* **2009**, *48*, 60−103.

(5) Pastoriza-Santos, I.; Liz-Marzán, L. M. *N,N*-Dimethylformamide as a Reaction Medium for Metal Nanoparticle Synthesis. *Adv. Funct. Mater.* **2009**, *19*, 679−688.

(6) Xiao, J.; Qi, L. Surfactant-Assisted, Shape-Controlled Synthesis of Gold Nanocrystals. *Nanoscale* **2011**, *3*, 1383−1396.

(7) Carbó-Argibay, E.; Rodríguez-González, B.; Pacifico, J.; Pastoriza-Santos, I.; Pérez-Juste, J.; Liz-Marzán, L. M. Chemical Sharpening of Gold Nanorods: The Rod-to-Octahedron Transition. *Angew. Chem., Int. Ed.* **2007**, *46*, 8983−8987.

(8) Sánchez-Iglesias, A.; Pastoriza-Santos, I.; Pérez-Juste, J.; Rodríguez-González, B.; García de Abajo, F. J.; Liz-Marzán, L. M. Synthesis and Optical Properties of Gold Nanodecahedra with Size Control. *Adv. Mater.* **2006**, *18*, 2529−2534.

(9) Ma, Y.; Li, W.; Cho, E. C.; Li, Z.; Yu, T.; Zeng, J.; Xie, Z.; Xia, Y. Au@Ag Core-Shell Nanocubes with Finely Tuned and Well-Controlled Sizes, Shell Thicknesses, and Optical Properties. *ACS Nano* **2010**, *4*, 6725−6724.

(10) Patra, P. P.; Pavan Kumar, G. V. Single-Molecule Surface-Enhanced Raman Scattering Sensitivity of Ag-Core Au-Shell Nanoparticles: Revealed by Bi-analyte Method. *J. Phys. Chem. Lett.* **2013**, *4*, 1167−1171.

(11) Xia, X.; Xia, Y. Symmetry Breaking during Seeded Growth of Nanocrystals. *Nano Lett.* **2012**, *12*, 6038−6042.

(12) Gong, J.; Zhou, F.; Li, Z.; Tang, Z. Synthesis of Au@Ag Core−Shell Nanocubes Containing Varying Shaped Cores and Their Localized Surface Plasmon Resonances. *Langmuir* **2012**, *28*, 8959−8964.

(13) Cardinal, M. F.; Rodríguez-González, B.; Alvarez-Puebla, R. A.; Pérez-Juste, J.; Liz-Marzán, L. M. Modulation of Localized Surface Plasmons and SERS Response in Gold Dumbbells Through Silver Coating. *J. Phys. Chem. C* **2010**, *114*, 10417−10423.

(14) Park, K.; Drummy, L. F.; Vaia, R. A. Ag Shell Morphology on Au Nanorod Core: Role of Ag Precursor Complex. *J. Mater. Chem.* **2011**, *21*, 15608−15618.

(15) Li, Q.; Jiang, R.; Ming, T.; Fang, C.; Wang, J. Crystalline Structure-Dependent Growth of Bimetallic Nanostructures. *Nanoscale* **2012**, *4*, 7070−7077.

(16) Park, K.; Drummy, L. F.; Wadams, R. C.; Koerner, H.; Nepal, D.; Fabris, L.; Vaia, R. A. Growth Mechanism of Gold Nanorods. *Chem. Mater.* **2013**, *25*, 548−554.
(17) Langille, M. R.; Personick, M. L.; Zhang, J.; Mirkin, C. A. Defining Rules for the Shape Evolution of Gold Nanoparticles. *J. Am. Chem. Soc.* **2012**, *134*, 14542−14554.
(18) Carbó-Argibay, E.; Rodríguez-González, B.; Gómez-Graña, S.; Guerrero-Martínez, A.; Pastoriza-Santos, I.; Pérez-Juste, J.; Liz-Marzán, L. M. The Crystalline Structure of Gold Nanorods Revisited. Evidence for Higher Index Lateral Facets. *Angew. Chem., Int. Ed.* **2010**, *49*, 9397.
(19) Goris, B.; Bals, S.; Van den Broek, W.; Carbó-Argibay, E.; Gómez-Graña, S.; Liz-Marzán, L. M.; Van Tendeloo, G. Atomic Scale Determination of Surface Facets in Nanocrystals. *Nat. Mater.* **2012**, *11*, 930−935.
(20) Johnson, C. J.; Dujardin, E.; Davis, S. A.; Murphy, C. J.; Mann, S. Growth and Form of Gold Nanorods Prepared by Seed-mediated, Surfactant-directed Synthesis. *J. Mater. Chem.* **2002**, *12*, 1765−1770.
(21) Nikoobakht, B.; El-Sayed, M. A. Preparation and Growth Mechanism of Gold Nanorods (NRs) Using Seed-Mediated Growth Method. *Chem. Mater.* **2003**, *15*, 1957.
(22) Okuno, Y.; Nishioka, K.; Kiya, A.; Nakashima, N.; Ishibashia, A.; Niidome, Y. Uniform and Controllable Preparation of Au−Ag Core−Shell Nanorods Using Anisotropic Silver Shell Formation on Gold Nanorods. *Nanoscale* **2010**, *2*, 1489−1493.
(23) Jiang, R.; Chen, H.; Shao, L.; Li, Q.; Wang, J. Unraveling the Evolution and Nature of the Plasmons in (Au Core)−(Ag Shell) Nanorods. *Adv. Mater.* **2012**, *24*, OP200−OP207.
(24) Jana, N. R.; Gearheart, L.; Murphy, C. J. Seed-Mediated Growth Approach for Shape-Controlled Synthesis of Spheroidal and Rod-like Gold Nanoparticles Using a Surfactant Template. *Adv. Mater.* **2001**, *13*, 1389−1393.
(25) Liu, M. Z.; Guyot-Sionnest, P. Mechanism of Silver(I)-Assisted Growth of Gold Nanorods and Bipyramids. *J. Phys. Chem. B* **2005**, *109*, 22192−22200.
(26) Liu, X.-H.; Luo, X.-H.; Lu, S.-X.; Zhang, J.-C.; Cao, W.-L. A Novel Cetyltrimethyl ammonium Silver Bromide Complex and Silver Bromide Nanoparticles Obtained by the Surfactant Counterion. *J. Colloid Interface Sci.* **2007**, *307*, 94−100.
(27) Hubert, F.; Testard, F.; Spalla, O. Cetyltrimethylammonium Bromide Silver Bromide Complex as the Capping Agent of Gold Nanorods. *Langmuir* **2008**, *24*, 9219−9222.
(28) Rodríguez-González, B.; Burrows, A.; Watanabe, M.; Kiely, C. J.; Liz-Marzán, L. M. Multishell Bimetallic AuAg Nanoparticles: Synthesis, Structure and Optical Properties. *J. Mater. Chem.* **2005**, *15*, 1755−1759.
(29) Xiang, Y.; Wu, X.; Liu, D.; Li, Z.; Chu, W.; Feng, L.; Zhang, K.; Zhou, W.; Xie, S. Gold Nanorod-Seeded Growth of Silver Nanostructures: From Homogeneous Coating to Anisotropic Coating. *Langmuir* **2008**, *24*, 3465−3470.
(30) Borsook, H.; Davenport, H. W.; Jeffreys, C. E. P.; Warner, R. C. The Oxidation of Ascorbic Acid and Its Reduction in Vitro and in Vivo. *J. Biol. Chem.* **1937**, *117*, 237−279.
(31) Gou, L.; Murphy, C. J. Fine-Tuning the Shape of Gold Nanorods. *Chem. Mater.* **2005**, *17*, 3668−3672.
(32) Magnussen, O. M. Ordered Anion Adlayers on Metal Electrode Surfaces. *Chem. Rev.* **2002**, *102*, 679−725.
(33) Wulff, G. On the Question of Speed of Growth and Dissolution of Crystal Surfaces. *Z. Krystallogr. Mineral.* **1901**, *34*, 449−530.
(34) Bamparis, G. D.; Remediakis, I. N. Dependence on CO Adsorption of the Shapes of Multifaceted Gold Nanoparticles: A Density Functional Theory. *Phys. Rev. B* **2012**, *86*, 085457-1−7.
(35) Pérez-Juste, J.; Liz-Marzán, L. M.; Carnie, S.; Chan, D. Y. C.; Mulvaney, P. Electric-Field-Directed Growth of Gold Nanorods in Aqueous Surfactant Solutions. *Adv. Funct. Mater.* **2004**, *14*, 571−579.
(36) Jana, N. R. Nanorod Shape Separation Using Surfactant Assisted Self-assembly. *Chem. Commun.* **2003**, 1950−1951.
(37) Kresse, G.; Hafner, J. Ab initio Molecular Dynamics for Liquid Metals. *Phys. Rev. B* **1993**, *47*, 558−561.
(38) Perdew, J. P.; Burke, K.; Ernzerhof, M. Generalized Gradient Approximation Made Simple. *Phys. Rev. Lett.* **1996**, *77*, 3865−3868.
(39) Kresse, G.; Joubert, D. From Ultrasoft Pseudopotentials to the Projector Augmented-Wave Method. *Phys. Rev. B* **1999**, *59*, 1758−1775.
(40) Neugebauer, J.; Scheffler, M. Adsorbate−Substrate and Adsorbate−Adsorbate Interactions of Na and K Adlayers on Al(111). *Phys. Rev. B* **1992**, *46*, 16067−16080.
(41) Gomez-Diaz, J.; Honkala, K.; Lopez, N. A Density Functional Theory Study on Gold Cyanide Interactions: The Fundamentals of Ore Cleaning. *Surf. Sci.* **2010**, *604*, 1552−1557.
(42) Marcus, Y. Thermodynamics of Solvation of Ions. Part 5.—Gibbs Free Energy of Hydration at 298.15 K. *J. Chem. Soc., Faraday Trans.* **1991**, *87*, 2995−2999.